PHYSICAL REVIEW B
CONDENSED MATTER

THIRD SERIES, VOLUME 35, NUMBER 16 1 JUNE 1987

Yield of photofield emitted electrons from tungsten

Y. Gao and R. Reifenberger
Purdue University, Department of Physics, West Lafayette, Indiana 47907
(Received 25 February 1986; revised manuscript received 24 November 1986)

An experimental determination of the yield of photofield emitted electrons from W(110) and W(111) for a number of different photon energies betwen 2.41 and 3.54 eV are reported. The measured yield is compared to a simple theoretical model of the photoexcitation process based on a step discontinuity at the metal-vacuum interface. A simple model for the spatial variation of the vector potential **A** near the metal-vacuum interface is also included. It is found that this model overestimates the yield by a factor of ~ 30 for W(110) and ~ 55 for W(111). This suggests that a self-consistent treatment of **A** is required to better understand the data.

I. INTRODUCTION

In photofield emission (PFE), a metal surface is illuminated by a laser beam of photon energy less than the work function Φ of the emitting surface. A strong electric field ($\sim 10^9$ V/m) is applied to the surface and permits electrons from both the photoexcited and ground states to tunnel through the surface potential barrier. Because these experiments measure the photocurrent produced by final states below the vacuum level, this technique is ideal for investigating basic aspects of photoexcitation over a range of low photon energies not accessible using other techniques.

The original motivation for investigating photofield emission focused on the possibility of obtaining joint density of states information.[1,2] Subsequent observations showed such effects are difficult to observe.[3–8] Recent work has revealed that the photofield emission current varies linearly with the incident photon flux, thereby indicating the dominance of a one photon photoexcitation process.[9] It has also been found that in PFE, initial-state effects can play an important role in determining the shape of the final-state energy distribution.[10,11]

The lack of dominant joint density-of-states effects suggests that a surface photoeffect is of considerable importance. This view is further supported by measurements of the photofield emitted current as a function of the polarization direction of the incident laser light.[10,12,13] A number of theoretical studies have also been reported which include the surface photoexcitation mechanism in photofield emission.[14–22] Caroli *et al.* emphasized the nonequilibrium aspect of PFE and discussed the process in terms of second-order perturbation theory.[14] Tarankо,[15–17] Bagchi,[18] and Schwartz[19–22] calculated photofield energy distributions assuming different surface potential barriers. A general characteristic of these theories is the triangular-shaped energy distribution which agrees reasonably well with experimental observation.

The growing evidence for a surface photoeffect in these experiments suggests that photofield emission may be a useful tool to further investigate the spatial variation of an electromagnetic field near metal surfaces. Kliewer's work on this subject shows a significant variation of the electromagnetic field in the surface region for frequencies below the plasma frequency.[23] Feibelman calculated self-consistently the variation of the vector potential **A** near a free-electron metal surface at higher photon energies.[24,25] According to his work, the variation becomes larger when the photon energy becomes smaller. The experiments reported below are designed to provide more information about the spatial variation of **A** at low photon energies.

In this paper we describe measurements of the yield of photofield emitted electrons from tungsten surfaces over a range of photon energies in the visible and near ultraviolet. The experimental results are compared to a model of PFE which includes a simplified treatment of the spatial variation of the electromagnetic field near a metal surface. At present, we are unable to include the complexity discussed in Refs. 23–25, and it is hoped that the presentation of this data will encourage further work in this area. It should be emphasized that the existing theories of photofield emission do not contain any adjustable parameters, thus allowing a quantitative check between the experimental photoyield and theoretical expectations.

The remainder of the paper is organized in the following way. The experimental considerations are described

in Sec. II. In Sec. III the theoretical background will be presented. Section IV contains the results and discussions. In Sec. V, we summarize the main conclusions obtained from this study.

II. EXPERIMENTAL APPARATUS

Most of the experimental apparatus used to measure the photofield emission energy distribution in this study have been described previously.[26–29] The incident laser beam is focused with a high-resolution mirror mount onto a tungsten field emitter through a quartz converging lens of focal length $f=350$ mm. The field emitter is enclosed in an UHV chamber ($P\leq 6\times 10^{-11}$ Torr) to prevent unwanted gas contamination of the surface. By adjusting a precision UHV manipulator, the emitter can be accurately aligned over the probe hole of an electron energy analyzer situated below the emitter. The signal received by a channeltron electron multiplier at the output of the analyzer is accumulated by an on-line PDP 11-23 computer which also controls a number of other experimental parameters.

The energy analyzer consists of a retardation analyzer and a 127° differential analyzer in tandem. The 127° analyzer has been enclosed in a high-permeability μ-metal shield to screen stray magnetic fields. The resolution of the analyzer has been estimated to be better than 70 meV.[29]

An argon-ion laser operating in the single line mode is used to illuminate the field emitter. The photon energies used in this study are therefore limited to the eight strongest emission lines from our laser. To minimize drifts in the laser output, the laser was operated in the light stabilization mode while taking data. Typically, a power flux density of about 10^8 W/m^2 is present at the field-emitter surface.

The size of the TEM_{00} incident laser beam was carefully determined at each wavelength by measuring the power intercepted by a knife edge as a function of the knife-edge position.[30] From this data, the beam diameter D, assuming a Gaussian intensity profile, can be determined for the different wavelengths λ. This was used to calculate the focused spot radius, ρ_0 of a laser beam passing through a lens of focal length f:

$$\rho_0=\frac{\lambda f}{\pi D} .$$

The field emission tips were prepared by electrochemical etching in $1N$ sodium hydroxide (NaOH) solution.[31] Typical clean field-emission patterns were observed and used, along with four deflection plates, to direct electrons emitted from W(110) and W(111) into the probe hole of the energy analyzer.

The field emitter can be cleaned *in situ* by passing a sufficient dc current through the supporting loop of the emitter. Since the electron emission and hence the photoelectron yield is sensitive to surface contamination, it becomes important to clean the field emitter reproducibly. In these experiments, this was attempted by using a timed flashing circuit that delivered a fixed current to the supporting loop for a preset period of time. In this way, the adsorbed gases from the tip could be removed in a reproducible fashion. In addition, all data were obtained from a well-annealed field emitter that had reached its equilibrium end form. Thus, even though the field emitter is momentarily raised to a high temperature between different data runs, the shape of the emitter did not change appreciably. Typical time for taking an energy distribution was about 10 min, a time sufficiently short to ensure that the surface contamination was below 0.05 monolayer by the end of a data run.

III. THEORETICAL CONSIDERATIONS

The matrix element M_{fi} that describes the photoexcitation of an electron from an initial state $|i\rangle$ to a final state $|f\rangle$ is given by

$$M_{fi}=\langle f \mid \mathbf{A}\cdot\mathbf{p}+\mathbf{p}\cdot\mathbf{A} \mid i\rangle , \tag{1}$$

where $\mathbf{A}$ is the vector potential of the radiation field of angular frequency ω in the gauge of zero scalar potential. Equation (1) can be rewritten as

$$M_{fi}=\frac{2i}{\hbar\omega}\left[\hbar\langle f \mid \mathbf{A}\cdot\nabla V \mid i\rangle+i\frac{\hbar^2}{2m}\langle f \mid \nabla^2\mathbf{A}\cdot\mathbf{p} \mid i\rangle - \frac{\hbar}{m}\langle f \mid \nabla(\mathbf{A}\cdot\mathbf{p})\cdot\mathbf{p} \mid i\rangle-\frac{\hbar^2\omega}{2}\langle f \mid \nabla\cdot\mathbf{A} \mid i\rangle\right], \tag{2}$$

where the commutator $\mathbf{A}\cdot\mathbf{p}$ with the Hamiltonian $H=p^2/2m+V$, given by

$$[\mathbf{A}\cdot\mathbf{p},H]=-i\hbar\mathbf{A}\cdot\nabla V+\frac{\hbar^2}{2m}\nabla^2\mathbf{A}\cdot\mathbf{p}+i\frac{\hbar}{m}\nabla(\mathbf{A}\cdot\mathbf{p})\cdot\mathbf{p} ,$$

has been used.

In order to compare the predictions of these matrix elements to experiment, we analyze them in a simplified way. Specific approximations include treating the emitting surface as a flat plane of large extent, even though the photoexcitation occurs from a facet, ~ 50 Å in extent, on a field emission tip of ~ 1000-Å radius. In what follows, the direction of the polarization vector is designated by $\hat{\epsilon}$. We assume a metal surface defined by an x-y plane and choose the plane of incidence to be the y-z plane. Thus the angle of incidence of the electromagnetic radiation is defined with respect to the positive z axis. It is also assumed that the surface potential V_s varies only along the surface normal $\hat{\mathbf{z}}$.

Using these approximations, the first matrix element in Eq. (2) is often conveniently written as

$$\langle f \mid \mathbf{A}\cdot\nabla V \mid i\rangle=\langle f \mid \mathbf{A}\cdot\nabla V_B \mid i\rangle+\langle f \mid \mathbf{A}\cdot\nabla V_S \mid i\rangle , \tag{3}$$

where ∇V_B and ∇V_S are the gradients of the bulk and surface potential participating in the photoexcitation of an electron. In the photofield emission process, the dominant contribution to the photocurrent comes from the surface photoeffect. Thus, the ∇V_B is not relevant to the measurements reported in this paper.

Under these conditions and writing $\mathbf{A}=A_0\hat{\epsilon}$, Eq. (3)

becomes

$$\langle f \mid \mathbf{A}\cdot\nabla V_s \mid i\rangle = \hat{\epsilon}\cdot\hat{\mathbf{z}}\left\langle f \left| A_0 \frac{dV_s}{dz} \right| i \right\rangle . \tag{4}$$

In photofield emission, the surface barrier V_s is deformed by the image potential $-e^2/4z$ and the applied electric field. However, the former varies rapidly only within ~ 2 Å from the surface. The latter is screened by surface charge located at the nominal metal surface. For the moment we neglect these two contributions to V_s and follow the simple approach suggested in Ref. 18, assuming a sharp interface such that $V_s(z)=V_0\Theta(z)$. Because of the rapid variation in both the image charge and electric field contribution to V_s at $z=0$, this approximation is not unreasonable.

This allows Eq. (4) to be further simplified to

$$\langle f \mid \mathbf{A}\cdot\nabla V_s \mid i\rangle = \hat{\epsilon}\cdot\hat{\mathbf{z}} A_0(0^-) V_0 \langle f(z=0) \mid i(z=0)\rangle , \tag{5}$$

where $A_0(0^-)$ is the magnitude of the vector potential just inside the metal surface. The $\hat{\epsilon}\cdot\hat{\mathbf{z}}$ polarization dependence exhibited in Eq. (4) may be altered by a real metal surface since the surface periodicity parallel to the surface will introduce extra terms in the evaluation of Eq. (4). These additional terms will depend on the x and y components of $\mathbf{A}$. If one can single these terms out, then a polarization-dependent study may provide a probe of the surface periodicity parallel to the metal surface.

The fourth matrix element in Eq. (2) is due to the spatial variation of the vector potential $\mathbf{A}$ in the vicinity of the metal surface and involves the evaluation of $\nabla\cdot\mathbf{A}$ near a metal surface. This term is important when the photon energy is less than the plasmon energy, and becomes larger, as the photon energy decreases.[32] Because the components of $\mathbf{A}$ parallel to the interface are expected to be continuous, it is assumed that $\nabla\cdot\mathbf{A}$ can be approximated at the metal-vacuum interface by

$$\nabla\cdot\mathbf{A} = \frac{\partial A_z}{\partial z} . \tag{6}$$

In the limit of a sharp interface and neglecting finite wavelength and nonlocal corrections, the variation in A_z is determined by a discontinuity at $z=0$, and Eq. (6) becomes

$$\nabla\cdot\mathbf{A} = \hat{\epsilon}\cdot\hat{\mathbf{z}} A_0(0^-)[\epsilon(\omega)-1]\delta(z) , \tag{7}$$

where $\epsilon(\omega)$ is the dielectric constant of the metal and $A_z(0^-)=\hat{\epsilon}\cdot\hat{\mathbf{z}} A_0(0^-)$ has been used. With these approximations, the matrix element in the fourth term in Eq. (2) can be written as

$$\langle f \mid \nabla\cdot\mathbf{A} \mid i\rangle = \hat{\epsilon}\cdot\hat{\mathbf{z}} A_0(0^-)[\epsilon(\omega)-1]\langle f(z=0) \mid i(z=0)\rangle . \tag{8}$$

Using the same model for evaluating $\nabla\cdot\mathbf{A}$, the matrix element of the second term of Eq. (2) can also be rewritten as

$$\langle f \mid \nabla^2 \mathbf{A}\cdot\mathbf{p} \mid i\rangle = -i\hbar(\hat{\epsilon}\cdot\hat{\mathbf{z}}) A_0(0^-)[\epsilon(\omega)-1]\left\langle f \left| \frac{\partial}{\partial z}\left[\delta(z)\frac{\partial}{\partial z}\right] \right| i \right\rangle . \tag{9}$$

The matrix element of the third term in Eq. (2) involves an evaluation of the operator $\nabla(\mathbf{A}\cdot\mathbf{p})\cdot\mathbf{p}$. Since the x and y components of $\mathbf{A}$ are continuous across the surface, and the variation of A_z in the x and y directions is negligible (the flat-surface approximation), this matrix element becomes

$$\langle f \mid \nabla(\mathbf{A}\cdot\mathbf{p})\cdot\mathbf{p} \mid i\rangle = (-i\hbar)^2 A_0(0^-)[\epsilon(\omega)-1]\hat{\epsilon}\cdot\hat{\mathbf{z}}\left\langle f \left| \delta(z)\frac{\partial^2}{\partial z^2} \right| i \right\rangle . \tag{10}$$

Each of these matrix elements can be further evaluated by assuming free electron initial- and final-state wave functions. Following Bagchi,[18] we use

$$|f\rangle = e^{ik_f z} , \tag{11}$$

where $\hbar^2(k_f^2/2m)=W+\hbar\omega$, and

$$|i\rangle = \sqrt{2}\sin(k_i z+\delta) , \tag{12}$$

with $\hbar^2(k_i^2/2m)=W$. Combining Eq. (2) with Eqs. (5) and (8)–(12), M_{fi} is now given by

$$M_{fi} = \frac{2i}{\hbar\omega}\hat{\epsilon}\cdot\hat{\mathbf{z}} A_0(0^-)\Gamma , \tag{13}$$

where

$$\Gamma = V_0\left[\frac{2W}{V_0}\right]^{1/2}\left[1-[\epsilon(\omega)-1]\left[\frac{\hbar\omega}{2V_0}+\frac{2W}{V_0}+i\frac{[(W+\hbar\omega)(V_0-W)]^{1/2}}{V_0}\right]\right] . \tag{14}$$

By defining Γ in this way, the contribution from the surface potential barrier [Eq. (4)] and from the spatial variation of $\mathbf{A}$ [last three terms in Eq. (14)] are clearly set out.

The effect of $\mathbf{A}$ operating on the photon part of the initial-state wave function must also be included. Since photoemission involves a photon-annihilation process, the appropriate numerical factors can be obtained through second quantization:

$$\langle n-1 \mid \mathbf{A} \mid n\rangle = \left[\frac{2\pi\hbar c^2}{\omega}\frac{n}{\Omega}\right]^{1/2} , \tag{15}$$

where n is the number of photons, Ω the normalization volume of the radiation field, and c the speed of light.

The matrix element M_{fi} can be used in a theory that predicts the energy distribution of photofield emitted elec-

trons. The current density per unit energy is given by[19]

$$\frac{dj}{dE} = -\frac{e^3}{2\hbar^4\omega^3}\frac{n}{\Omega}(\hat{\epsilon}\cdot\hat{z})^2 f(E-\hbar\omega) \times \int_{-V_0+\hbar\omega}^{E} dW \frac{D(W)\,|\,\Gamma\,|^2}{[W(W-\hbar\omega)]^{1/2}} . \quad (16)$$

Other quantities in Eq. (16) have their usual definitions. $f(E-\hbar\omega)$ is the Fermi-Dirac distribution function shifted upward by the energy of the incident photons. $D(W)$ is the transmission probability which describes the quantum-mechanical transmission probability that photoexcited electrons with energy $E=(\hbar k)^2/2m+W$ will traverse the surface potential barrier deformed by the applied electrostatic field and the static image potential barrier.[33]

The photon density inside the metal contributing to the photoexcitation process can be approximated by

$$\frac{n}{\Omega}(\hat{\epsilon}\cdot\hat{z})^2 = \frac{P}{\hbar\omega}\frac{1}{\pi\rho_0^2 c}\left|\frac{A_z(0^-)}{A_0}\right|^2 , \quad (17)$$

where P is the incident laser power, ρ_0 is the radius of the focused laser beam defined in Sec. II, and the ratio of $A_z(0^-)$ to A_0 describes the fraction of photons penetrating the surface and producing the photofield current. The evaluation of Eq. (17) requires a model for the vector potential in the vicinity of the metal surface. In this paper, we use the Fresnel model to estimate $A_z(0^-)$:

$$\frac{A_z(0^-)}{A_0} = \frac{\sin(2\theta_i)}{[\epsilon(\omega)-\sin^2(\theta_i)]^{1/2}+\epsilon(\omega)\cos(\theta_i)} , \quad (18)$$

where θ_i is the incident angle and $\epsilon(\omega)$ is the dielectric constant.

The yield can be calculated by integrating dj/dE of Eq. (16) and then dividing the result by n/Ω. In order to compare this quantity to experimental data, it is useful to first normalize it by the field-emission current calculated using a free-electron model:[34–36]

$$\left[\frac{dj}{dE}\right]_{fe} = \frac{J_0}{d} f(E) e^{(E-E_F)/d} , \quad (19)$$

where

$$J_0 = \frac{4\pi med^2}{h^3} e^{-c}, \quad c = 4\frac{(2m\Phi^3)^{1/2}}{3\hbar eF} v(y) , \quad d = \frac{\hbar eF}{2(2m\Phi)^{1/2} t(y)}, \quad y = \frac{(e^3F)^{1/2}}{\Phi} , \quad (20)$$

and $t(y)$ and $v(y)$ are well-known elliptic functions.[37] The relative yield Y_r is then defined as

$$Y_r = \frac{\int (dj/dE)dE}{\int (dj/dE)_{fe} dE} . \quad (21)$$

In order to facilitate future calculations of Y_r to our experimental data, the data were normalized to a free-space photon density $(n/\Omega)_n = 10^9/4.8\pi$ cm^{-3}. This is the number of 1-eV photons in a 1-W laser beam with a uniform radius $\rho_0 = 1$ cm. Since a typical focal spot size in our experiments is characterized by ρ_0 of about 40×10^{-4} cm, the measured values of Y_r will be larger by a factor of order 10^5 for our experimental conditions. This factor, which was evaluated from our measurements of P, ω, and ρ_0, was divided out of our measurements before comparing experimental data to Eq. (21).

Dividing the photofield emission current by the field emission current removes difficulties involved in determining the exact area from which the electrons are emitted, since the measured photofield and field emission currents involve the same area and the division cancels this unknown factor. In addition, the sensitivity of the final results to the work function Φ and the electric field strength F are greatly reduced because uncertainties in these two quantities affect both the field emission and photofield emission energy distributions and hence tend to cancel when the ratio defined in Eq. (21) is formed. In addition, the above method reduces the effects of initial state structure since this structure influences both the numerator and denominator in Eq. (21). In principle, the above definition for Y_r contains no adjustable parameters, since all parameters can be determined from experiment.

IV. RESULTS AND DISCUSSIONS

Figure 1 shows a typical electron-energy distribution from W(110), obtained when $\hbar\omega$ is 2.71 eV and the field is 3.1×10^9 V/m. The field is determined using the well-known Fowler-Nordheim plot. The light is p polarized and the incident angle is 70° from the surface normal. Two distributions can be seen from the figure. The distribution near E_F is due to field-emitted electrons [Eq. (19)]. The distribution at higher energies, located near $E_F+\hbar\omega$, is due to photoexcited electrons [Eq. (16)]. Both curves were obtained during a single data acquisition run so that identical electric field and work functions are influencing each distribution. These energy distributions can be compared to the expected relative yield Y_r by numerically calculating the area under these two curves and forming the appropriate ratio.

Photofield energy distributions from W(110) with pho-

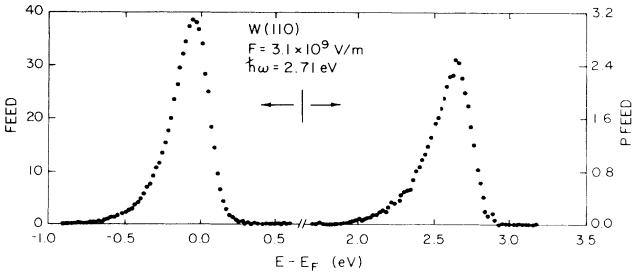

FIG. 1. Experimental field emission (FEED) and photofield (PFEED) energy distributions from W(110) for $\hbar\omega=2.71$ eV and for an applied electric field strength of $F=3.1\times10^9$ V/m. The field emission signal was used to determine the strength of the applied field as well as the temperature rise of the laser-illuminated tip. In addition, the field emission signal provided a convenient normalization of the photofield signal to reduce the large effects of small changes in the work function and applied electric field strength.

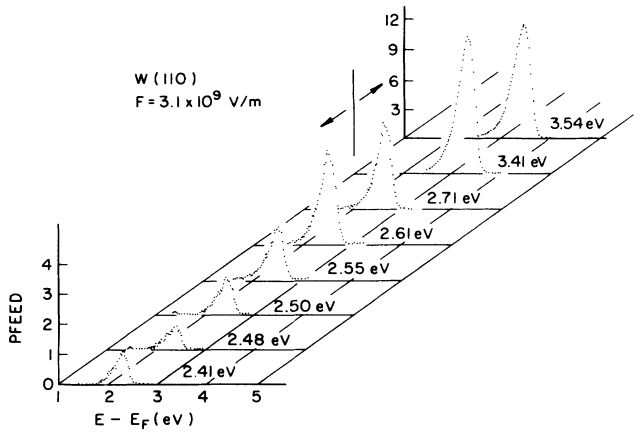

FIG. 2. Photofield energy distributions from W(110) as a function of photon energy in an electric field $F = 3.1 \times 10^9$ V/m.

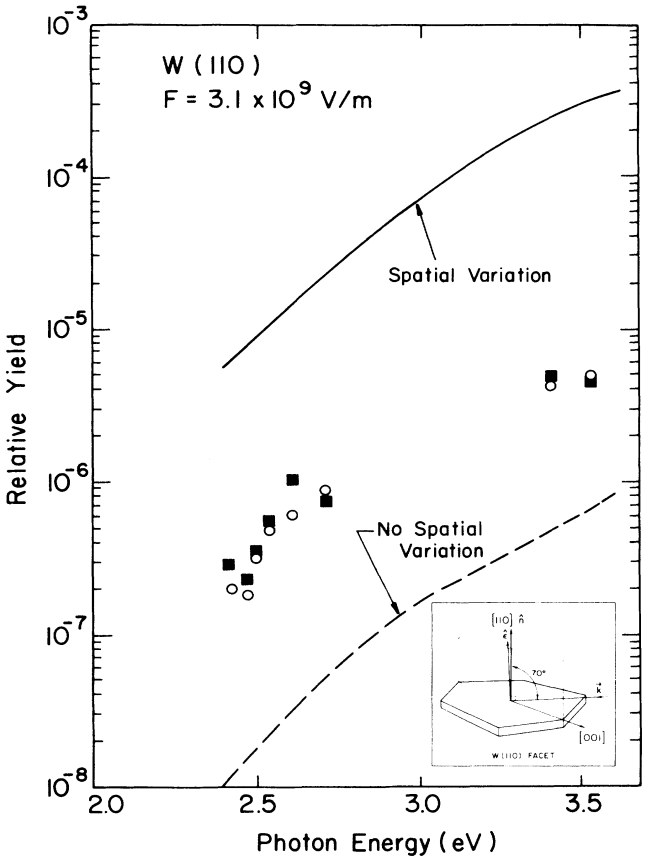

FIG. 3. Relative photofield yield Y, from W(110) as a function of photon energy. The circles and squares represent data taken on two different days. The solid line is the expected photoyield including the spatial variation of the **A**. The dashed line neglects this contribution to the photofield current. The experimental data have been normalized in order to compare to the normalized photon density discussed in the text. The inset shows the geometry of the incident laser beam. The incident light, characterized by **k**, is confined to the plane of incidence as shown. The wave vector **k** makes a 70° angle of incidence to the [110] surface normal directed along $\hat{\mathbf{n}}$.

ton energies from 2.41 to 3.54 eV are shown in Fig. 2 for a fixed electric field of 3.1×10^9 V/m. The incident angle and polarization of the light are the same as that in Fig. 1. Between the accumulation of each energy distribution, the tip was cleaned and the focal spot was carefully optimized to provide the maximum photocurrent. This involved a careful repositioning of the quartz focusing lens in order to correct for its wavelength-dependent index of refraction. As the photon energy increases, the width of the distribution also increases since the transmission probability near the vacuum level is slowly approaching unity.[33]

The relative yields obtained by integrating the photofield energy distributions in Fig. 2 are shown in Fig. 3 as solid squares. The focal spot size and laser beam power were incorporated in scaling the yields from

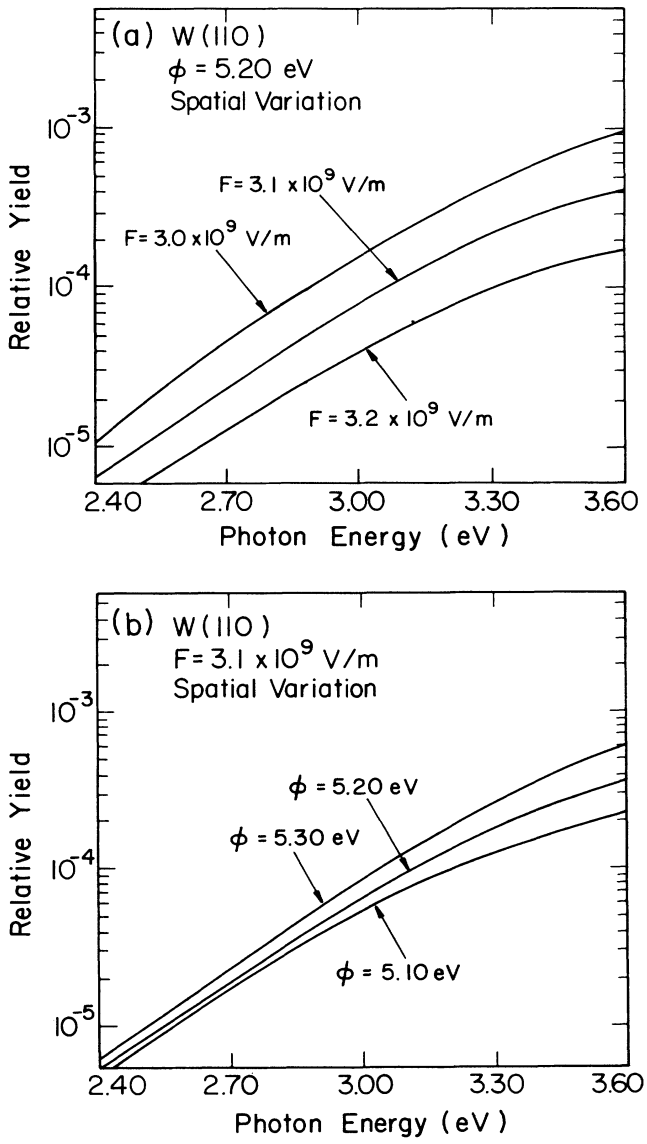

FIG. 4. An illustration of the effect of a small change in electric field strength (a) and work function (b) on the calculated photofield yield for W(110). The calculations shown include the spatial variation of **A**.

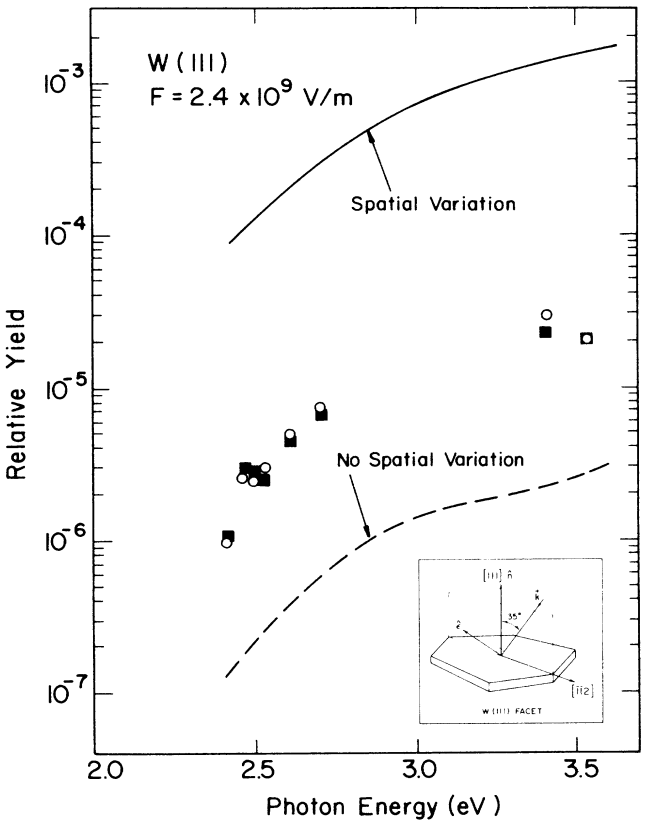

FIG. 5. Relative photofield yield Y_r from W(111) as a function of photon energy. The circles and squares represent data taken on two different days. The solid line is the expected photoyield including the spatial variations of **A**. The dashed line neglects this contribution to the photofield current. The experimental data have been normalized in order to compare to the normalized photon density discussed in the text. The inset shows the geometry of the incident laser beam. The incident light, characterized by **k**, is confined to the plane of incidence as shown. The wave vector **k** makes a 35° angle of incidence to the [111] surface normal directed along $\hat{\mathbf{n}}$.

different wavelengths to the standard photon density discussed in Sec. III. An independent set of data taken at another time is also shown in Fig. 3 as open circles. The difference between the two data sets are due to a number of reasons, one of which is the difficulty in optimizing the focal spot of the laser on the field emitter. In addition, a slight change in the surface condition induced by the tip cleaning procedure cannot be ruled out. Since the field emitter was always flashed above 2000 °C before taking an energy distribution to remove any surface adsorbates, small surface rearrangements which influence the microscopic work function and electric field strength must inevitably take place. Nonetheless, the data seem sufficiently well characterized to allow a comparison to theoretical expectations.

The two curves shown in Fig. 3 are theoretical results calculated using Eq. (21). The geometry of the incident light is shown in the inset of Fig. 3. The solid curve includes the terms due to the spatial variation of **A** while the dashed one does not. The surface barrier height V_0 is measured from the conduction-band bottom to the vacuum level, which is taken to be 10.8 eV.[19] The work function of the surface $\Phi = 5.2$ eV is taken from the literature.[38] The temperature rise of the field emitter (about 100 °C) under laser illumination was determined from the leading edge of the measured field emission distributions as described in another publication.[39] Experimental dielectric constants tabulated in Ref. 40 were used in evaluating A_z from Eq. (18).

The yield is sensitive to the electrostatic field and work function, and these two parameters are known only to limited accuracies. We plot the theoretical curves assuming reasonable uncertainties in these two parameters in Fig. 4. It can be seen that neither the uncertainty in the electric field [Fig. 4(a)], nor the work function [Fig. 4(b)], have important effects.

The relative photoyield from W(111) is plotted in Fig. 5. The incident light is p polarized and the geometry is shown in the inset of Fig. 5. Theoretical curves based on the model discussed in Sec. III are also illustrated in the figure. The parameters in the calculations were identical to those used for W(110) except that Φ for W(111) was taken to be 4.4 eV.[38]

V. CONCLUSIONS

In this paper, measurements of photofield emission yields from W(110) and W(111) as a function of photon energy from 2.41 to 3.54 eV are reported. The data are compared to a simplified model of the photofield emission process which includes the surface photoelectric effect. The theoretical calculations bracket the experimental data. The yield calculated on the basis of Eq. (13) overestimates the data by a factor of ~ 30 for W(110) and ~ 55 from W(111). Calculations neglecting the spatial variation of **A** underestimate the data by a factor of ~ 20 for W(110) and ~ 13 for W(111). It is not yet clear whether more complete theories of the $\nabla \cdot \mathbf{A}$ term will remove this discrepancy.

ACKNOWLEDGMENTS

The work was supported by U.S. Department of Energy Contract No. DE45162. One of us (Y.G.) would like to thank the David Ross Foundation for financial support. The authors would like to thank W. L. Schaich for useful comments on the manuscript prior to publication.

[1]H. Newmann, Physica **44**, 1193 (1969).
[2]B. I. Lundqvist, K. Mountfield, and J. W. Wilkins, Solid State Commun. **10**, 383 (1972).
[3]M. J. G. Lee, Phys. Rev. Lett. **30**, 1193 (1973).
[4]T. Radon and Ch. Kleint, Surf. Sci. **60**, 540 (1976).
[5]R. Reifenberger, H. A. Goldberg, and M. J. G. Lee, Surf. Sci. **83**, 599 (1979).
[6]D. Venus and M. J. G. Lee, Phys. Rev. B **28**, 437 (1983).

[7]R. Reifenberger, C. M. Egert, and D. L. Haavig, J. Vac. Sci. Technol. A **2**, 927 (1984).
[8]D. L. Haavig and R. Reifenberger, Surf. Sci. **151**, 128 (1985).
[9]D. Venus and M. J. G. Lee, Surf. Sci. **116**, 359 (1982).
[10]Y. Gao and R. Reifenberger, Phys. Rev. B **32**, 1380 (1985).
[11]D. Venus and M. J. G. Lee, Rev. Sci. Instrum. **56**, 1206 (1985).
[12]Y. Teisseyre, R. Haug, and R. Coelho, Surf. Sci. **87**, 549 (1979).
[13]D. Venus and M. J. G. Lee, Surf. Sci. **125**, 452 (1983).
[14]C. Caroli, D. Lederer-Rozenblatt, B. Roulet, and D. Saiht-James, Phys. Rev. B **10**, 10 (1973).
[15]E. Taranko, Acta Phys. Pol. A **49**, 721 (1976).
[16]E. Taranko, J. Phys. **38**, 163 (1977).
[17]E. Taranko, Acta Phys. Pol. A **53**, 761 (1978).
[18]A. Bagchi, Phys. Rev. B **10**, 542 (1974).
[19]C. Schwartz, Ph.D. thesis, Pennsylvania State University, 1980.
[20]C. Schwartz and M. W. Cole, Surf. Sci. **95**, L243 (1980).
[21]C. Schwartz and W. L. Schaich, Phys. Rev. B **24**, 1583 (1981).
[22]C. Schwartz and M. W. Cole, Surf. Sci. **115**, 290 (1982).
[23]K. L. Kliewer, Phys. Rev. B **14**, 1412 (1976); **15**, 3759 (1977).
[24]P. J. Feibelman, Phys. Rev. B **12**, 1319 (1975).
[25]P. J. Feibelman, Phys. Rev. B **14**, 762 (1976).
[26]C. M. Egert and R. Reifenberger, Surf. Sci. **145**, 159 (1984).
[27]D. L. Haavig and R. Reifenberger, Surf. Sci. **151**, 128 (1985).
[28]Y. Gao and R. Reifenberger, Phys. Rev. B **35**, 6627 (1987).
[29]Y. Gao and R. Reifenberger, J. Phys. E **18**, 381 (1985).
[30]M. J. G. Lee, R. Reifenberger, E. S. Robins, and H. G. Lindenmayr, J. Appl. Phys. **51**, 4996 (1980).
[31]A. J. Melmed and J. J. Carroll, J. Vac. Sci. Technol. A **2**, 1388 (1984).
[32]K. L. Kliewer, in *Photoemission and the Electronic Properties of Solids,* edited by B. Feuerbacher, B. Fitton, and R. F. Willis (Wiley, New York, 1978); H. J. Levinson, E. W. Plummer, and P. J. Feibelman, J. Vac. Sci. Technol. **17**, 216 (1980).
[33]R. Reifenberger, D. L. Haavig, and C. M. Egert, Surf. Sci. **109**, 276 (1981).
[34]R. H. Fowler and L. W. Nordheim, Proc. R. Soc. London, Ser. A **199**, 173 (1928).
[35]R. H. Good and E. W. Muller, in *Handbuch der Physik,* edited by S. Flügge (Springer-Verlag, Berlin, 1956).
[36]J. W. Gadzuk and E. W. Plummer, Rev. Mod. Phys. **45**, 487 (1973).
[37]H. Craig Miller, J. Vac. Sci. Technol. **17**, 691 (1980).
[38]T. V. Vorburger, D. Penn, and E. W. Plummer, Surf. Sci. **48**, 417 (1978).
[39]Y. L. Gao and R. Reifenberger, J. Vac. Sci. Technol. A **4**, 1289 (1986).
[40]J. H. Weaver, C. Krafka, D. W. Lynch, and E. E. Koch, *Physik Daten* (Fachinformationszentrum, Karlsruhe, 1981), Vol. 18-1.